

O VI and Multicomponent H I Absorption Associated with a Galaxy Group in the Direction of PG0953+415: Physical Conditions and Baryonic Content^{1,2}

Todd M. Tripp³ and Blair D. Savage⁴

ABSTRACT

We report the discovery of an O VI absorption system at $z_{\text{abs}} = 0.14232$ in a high resolution FUV spectrum of PG 0953+415 obtained with the Space Telescope Imaging Spectrograph (STIS). Both lines of the O VI $\lambda\lambda$ 1032, 1038 doublet and multicomponent H I Ly α absorption are detected, but the N V doublet and the strong lines of C II and Si III are not apparent. We examine the ionization mechanism of the O VI absorber and find that while theoretical considerations favor collisional ionization, it is difficult to observationally rule out photoionization. If the absorber is collisionally ionized, it may not be in equilibrium due to the rapid cooling of gas in the appropriate temperature range. Non-equilibrium collisionally ionized models are shown to be consistent with the observations. A WIYN survey of galaxy redshifts near the sight line has revealed a galaxy at a projected distance of 395 kpc separated by ~ 130 km s⁻¹ from this absorber, and three additional galaxies are found within $\lesssim 130$ km s⁻¹ of this redshift with projected separations ranging from 1.0 Mpc to 3.0 Mpc. All of these galaxies are luminous ($0.6 - 4.0 L_*$), and two of them show the [O II] $\lambda 3727$ emission line indicative of active star formation. The galaxies with

¹Based on observations obtained with the WIYN Observatory, which is a joint facility of the University of Wisconsin, Indiana University, Yale University, and the National Optical Astronomy Observatories.

²Based on observations with the NASA/ESA *Hubble Space Telescope*, obtained at the Space Telescope Science Institute, which is operated by the Association of Universities for Research in Astronomy, Inc., under NASA contract NAS 5-2555.

³Princeton University Observatory, Peyton Hall, Princeton, NJ 08544, Electronic mail: tripp@astro.princeton.edu

⁴Department of Astronomy, University of Wisconsin - Madison, 475 N. Charter St., Madison, WI 53706 - 1582, Electronic mail: savage@astro.wisc.edu

[O II] emission are probably normal spirals. Combining the STIS observations of PG0953+415 with previous high signal-to-noise observations of H1821+643 with the Goddard High Resolution Spectrograph (GHRS), we find two O VI systems with $W_r > 60 \text{ m\AA}$ and $z < 0.3$ over a total redshift path Δz of only 0.10. Both of these QSOs were originally observed to study the low z Ly α lines and should not be biased in favor of O VI detection. If these sight lines are representative, they imply a large number of O VI absorbers per unit redshift, $dN/dz \sim 20$. The corresponding value of dN/dz for low z Ly α lines with $W_r > 50 \text{ m\AA}$ is 102 ± 16 . We use this sample to obtain a first estimate of the cosmological mass density of the O VI systems at $z \approx 0$. If further observations confirm the large dN/dz derived for the O VI systems, then these absorbers trace a significant reservoir of baryonic matter at low redshift.

Subject headings: cosmology: observations — galaxies: halos — intergalactic medium — quasars: absorption lines — quasars: individual (PG0953+415)

1. Introduction

Hydrodynamic simulations of cosmological structure growth predict that when the initial density perturbations collapse, gas should be shock-heated to temperatures of $10^5 - 10^7 \text{ }^\circ\text{K}$ (Ostriker & Cen 1996; Davé et al. 1999; Cen & Ostriker 1999a). The fraction of the gas which has been heated to these temperatures increases with decreasing redshift, and at the present epoch, the model of Cen & Ostriker (1999a) predicts that 47 % of the baryons (by mass) are in this shock-heated phase, hereafter referred to as warm/hot gas (to distinguish it from the hotter gas in rich galaxy clusters which are readily detected X-ray sources). This warm/hot gas prediction has not been adequately tested by observations because the soft X-rays emitted by gas at these temperatures are difficult to detect with current instrumentation, especially at lower temperatures where corrections for foreground absorption and emission are complicated. However, it may be possible to detect gas in the lower half of this temperature range via absorption lines of species such as O VI, Ne VIII, or Mg X in the spectrum of a background QSO (Verner, Tytler, & Barthel 1994). It is important to search for this warm/hot gas as part of the census of matter in the universe and because it could affect the formation and evolution of galaxies and galaxy groups and clusters (e.g., Blanton et al. 2000).

There are some indications that warm/hot gas is present in some galaxy groups. For example, Mulchaey et al. (1996) have noted that ROSAT observations show that poor

galaxy groups which are rich in elliptical galaxies tend to exhibit X-ray emission ($E > 0.5$ keV) while spiral-rich groups do not. They suggest that spiral-rich groups contain cooler ($\lesssim 4 \times 10^6$ K) intragroup gas which is not easily detected in X-rays, and they predict that the intragroup medium of spiral-rich groups will produce absorption lines of O VI, but not C IV or N V because their column densities are too low at $T > 5 \times 10^5$ °K. Interestingly, Savage, Tripp, & Lu (1998) have recently identified a QSO absorber in the spectrum of H1821+643 ($z_{\text{QSO}} = 0.297$) which fits this description: O VI absorption lines with two nearby spiral galaxies but no accompanying C IV or N V lines. However, the absorption could be due to the halo of the closer spiral galaxy (which is at a projected distance of $105 h_{75}^{-1}$ kpc) rather than the intragroup medium, and Savage et al. show that the O VI absorption could plausibly arise in very low density photoionized gas. The O VI doublet has been identified in several other intervening absorption systems⁵ both at moderate redshifts (e.g., Bergeron et al. 1994; Burles & Tytler 1996; Jannuzi et al. 1998; Lopez et al. 1999; Churchill & Charlton 1999) and at high redshifts (Kirkman & Tytler 1997,1999). Composite spectra and statistical techniques have also been used to show that O VI absorption is present at high z (Lu & Savage 1993; Davé et al. 1998). In most cases it has been difficult to pin down the ionization mechanism definitively, partly due to the low resolution of the observations made with first-generation *Hubble Space Telescope* (*HST*) spectrographs, but in several cases there is evidence that the O VI systems occur in multiphase absorbing media. An important step in this approach to the search for warm/hot gas is to determine whether the O VI absorbers trace collisionally ionized gas or photoionized gas.

As part of the program described by Tripp, Lu, & Savage (1998) to study low z Ly α absorption line systems, we have recently observed the low redshift QSO PG0953+415 ($z_{\text{QSO}} = 0.239$) with the E140M echelle mode of the Space Telescope Imaging Spectrograph (STIS). This high resolution FUV spectrum has revealed another highly ionized O VI absorber associated with a group of spiral galaxies, and in this paper we present our analysis of this particular absorbing system. In §2 we review the observations and data reductions including measurements of galaxy redshifts with the WIYN telescope. We present in §3 the absorption line measurements. We constrain the temperature of the gas and examine its ionization in §4, and we discuss the implications of the observations in §5. Throughout this paper we assume $H_0 = 75h_{75}$ km s⁻¹ Mpc⁻¹ and $q_0 = 0.0$. Also, all wavelengths and

⁵Strong O VI absorption lines have also been detected in “associated” absorption line systems with $z_{\text{abs}} \approx z_{\text{QSO}}$ (e.g., Papovich et al. 2000 and references therein). These are a rather different class of absorber which are often known to be very close to the QSO (Hamann & Ferland 1999). In this paper, we have focused our analysis and discussion on the intervening systems.

redshifts reported here are heliocentric, but in this direction heliocentric and LSR velocities are nearly identical.⁶

2. Observations

2.1. STIS Spectroscopy of PG 0953+415

PG 0953+415 was observed with STIS on 1998 December 4 and 1998 December 11 resulting in a total integration time of 24478 seconds.⁷ The observations were obtained with the medium resolution FUV echelle mode (E140M) with the 0.2×0.2” aperture. Kimble et al. (1998) report that this STIS mode provides a resolution of $R = \lambda/\Delta\lambda = 46000$ (FWHM $\approx 7 \text{ km s}^{-1}$) with the 0.2×0.06” slit. With the 0.2×0.2” slit, the FWHM is nearly identical but the broad wings of the line spread function are stronger (see Figure 13.87 in the Cycle 9 STIS Instrument Handbook). Photoevents were recorded by the FUV-MAMA detector in accumulation mode with on-board orbital Doppler compensation, and individual exposures ranged from 2215 to 2880 seconds in duration. Short exposures of a wavelength calibration lamp were obtained with each individual observation of the QSO.

The data were reduced with the software developed by the STIS Instrument Definition Team (IDT). Pixel-to-pixel sensitivity variations in the individual exposures were first corrected with a postlaunch flatfield, and then the individual images were aligned by cross-correlation⁸ and then coadded. To prolong the lifetime of the MAMA detector, the position of the dispersed spectrum on the detector is changed every few weeks. This was done between the first observation of PG 0953+415 and the second, which is beneficial because when the data are aligned and coadded, any residual fixed-pattern noise not adequately removed by the flatfield is reduced. This also enables the identification of

⁶Assuming the Sun is moving in the direction $l = 53^\circ, b = 25^\circ$ at 16.5 km s^{-1} (Mihalas & Binney 1981), $v_{\text{LSR}} = v_{\text{helio}} - 0.1 \text{ km s}^{-1}$.

⁷The QSO was observed for 10743 seconds on December 4 (*HST* archive ID no. O4X002010) and for 13735 seconds on December 11 (*HST* archive ID nos. O4X001010 and O4X001020).

⁸The images can be aligned by cross-correlating the target images or the corresponding wavelength calibration lamp images. In principle direct cross-correlation of the target images is preferred because drift of the target in the aperture could cause shifts derived from the comparison lamp exposures to differ from the shifts appropriate for the target exposures. However, in this case the target images must contain enough sharp features to produce a sharp peak in the cross-correlation. We tried both methods, and we found that for this QSO observation, slightly better resolution was always obtained by cross-correlating the wavelength lamp exposures to determine the image shifts.

spurious features by comparison of the wavelength-calibrated spectra obtained on the two occasions. After coaddition of the individual images, the scattered light correction described by Bowers and Lindler (1999) was applied. Then the spectra from each order were extracted with a simple unweighted slit with the standard height of 11 “lores” pixels,⁹ and smoothing of the background region also followed standard procedures for the STIS echelle modes. During the extraction, obviously hot pixels were fixed by interpolation between the adjacent pixels in the dispersion direction. The wavelength scale was computed with a postlaunch dispersion relation (which is updated when the position of the spectrum on the detector is changed) and put on a heliocentric basis. Finally, the data were flux calibrated and overlapping regions of adjacent orders were coadded with weighting based on signal-to-noise (S/N). The wavelength coverage is $\sim 1150\text{--}1730$ Å with 5 small gaps between orders at $\lambda > 1630$ Å.

Samples of the final spectrum are shown in Figure 1. We identify the lines at 1178.8 and 1185.3 Å as the O VI $\lambda\lambda 1032, 1038$ doublet at $z_{\text{abs}} = 0.14232$, and the corresponding H I Ly α line is well-detected at 1388.7 Å. A marginal absorption line is apparent at the expected wavelength of Ly β as well, but it is recorded in a region where the spectrum is quite noisy. Note that the Ly α profile shows several components, the strongest of which is well-aligned with the O VI lines. There are no convincing alternative identifications of these lines. They are unlikely to be due to the ISM of the Milky Way since there are no resonance absorption lines at these wavelengths (see Morton 1991). The lines at 1178.8 and 1185.3 Å cannot be Ly β , γ , or δ lines due to extragalactic absorption systems at different redshifts because the corresponding Ly α lines are not detected at the expected wavelengths. Similarly, we have searched for alternative metal line identifications at other redshifts, and we find no convincing candidates.

Since the O VI doublet was recorded in a spectral region which is relatively noisy, and since there are slightly hot spurious pixels apparent in this portion of the spectrum (see Figure 1), we inspected the spectra obtained on December 4 and December 11 independently to confirm that the O VI lines are real. Both O VI lines are detected in the individual December 4 and December 11 spectra, and the relative line depths and wavelength difference of the lines are consistent with the O VI identification. However, we noticed that the O VI $\lambda 1037.6$ line is broader in the December 4 spectrum than the December 11 spectrum. For the reader’s inspection, Figure 2 compares the O VI $\lambda 1037.6$ profiles derived from the 1998 December 4 and 1998 December 11 data and from all of the

⁹The MAMAs are designed to support half-pixel centroiding (see Timothy 1994), and these half-pixels are usually referred to as “hires” pixels. This capability was not employed here since it does not enhance the data for this particular observation.

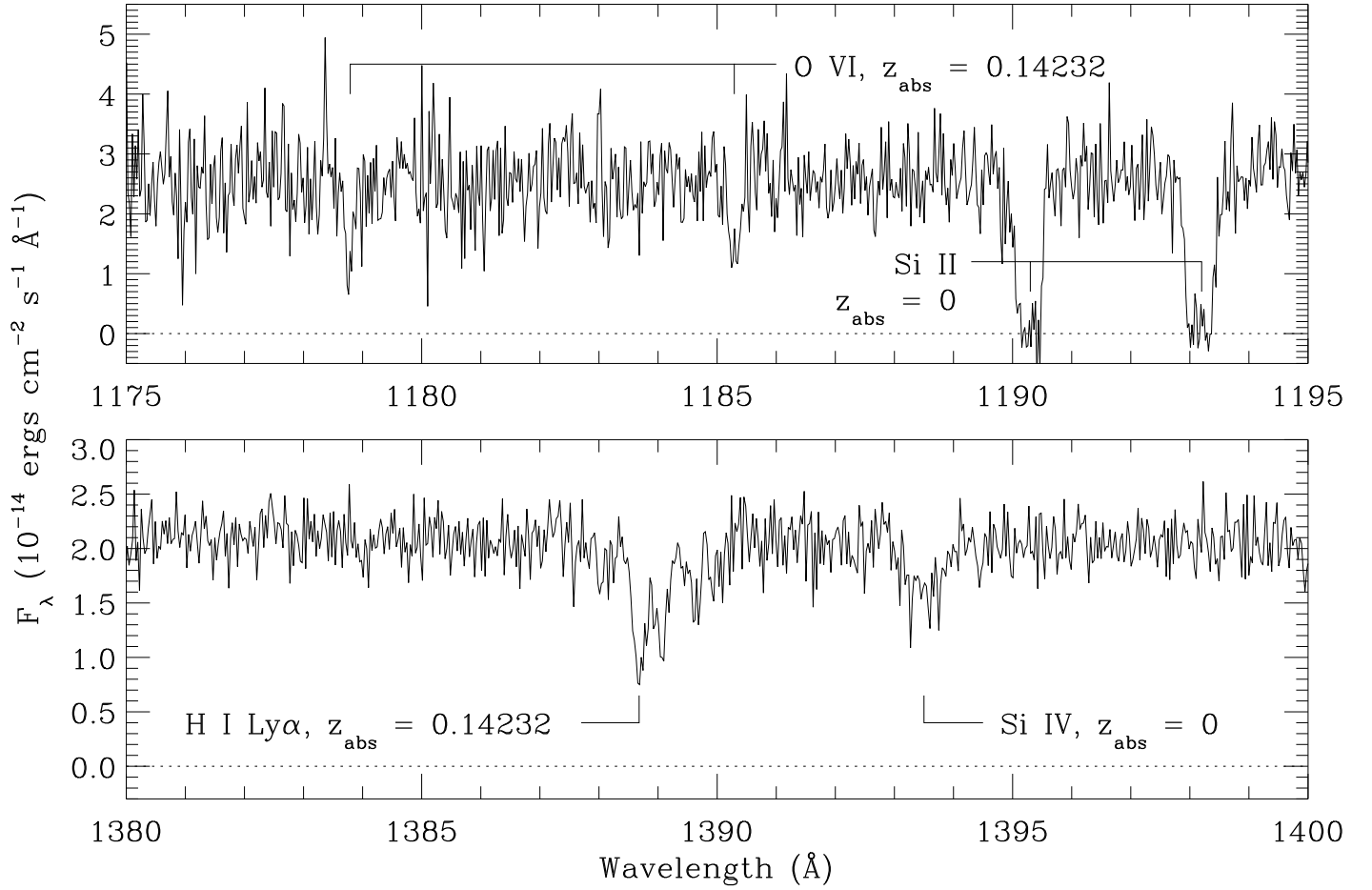


Fig. 1.— Portions of the STIS spectrum of PG 0953+415 obtained with the intermediate resolution FUV echelle mode (E140M). The O VI $\lambda\lambda 1032, 1038$ lines and the H I Ly α line at $z_{\text{abs}} = 0.14232$ are marked. Unrelated Milky Way lines in the selected regions are also indicated. In this figure, the data have been binned two pixels into one for display purposes only (i.e., all measurements in the tables and text were made using the full resolution unbinned data).

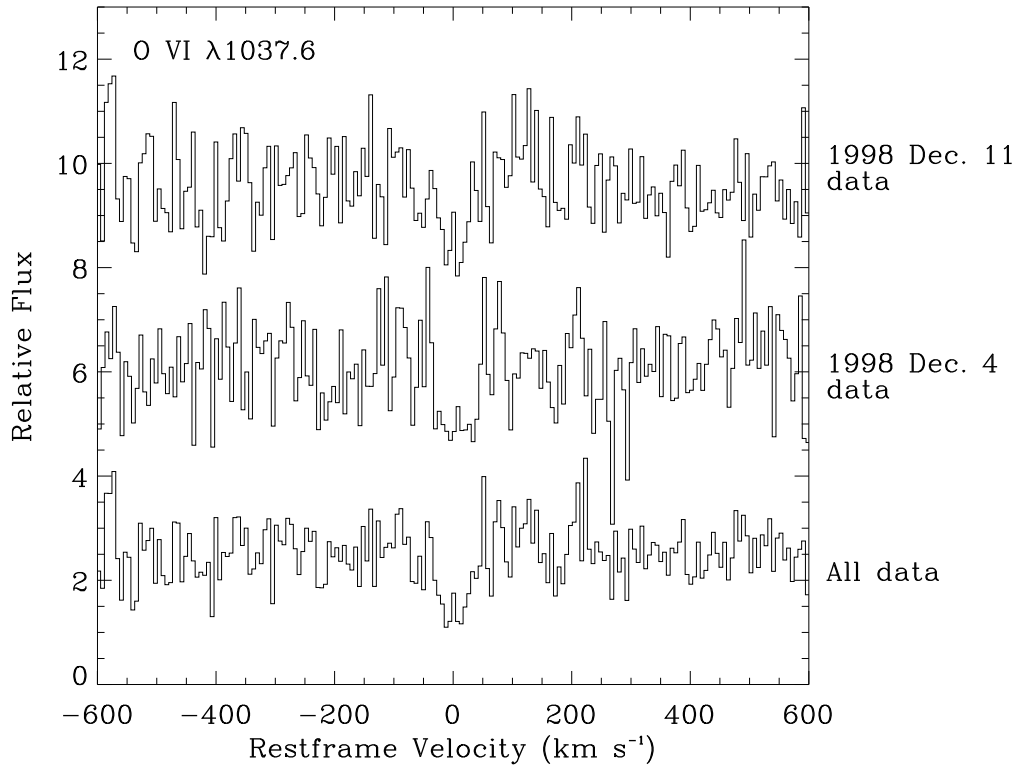


Fig. 2.— Comparison of the O VI $\lambda 1037.6$ profile at $z_{\text{abs}} = 0.14232$ in the data obtained on 1998 December 11 (upper spectrum), on 1998 December 4 (middle spectrum), and in all of the data combined (lower spectrum). The spectra are plotted versus restframe velocity where $v = 0$ at $z_{\text{abs}} = 0.14232$ and are offset for clarity. As in Figure 1, the data have been binned two pixels into one.

data combined. We suspect that the 1037.6 Å line is broader in the December 4 spectrum due to noise, perhaps due to fixed pattern noise which was not adequately removed by the flatfield available when the data were reduced. Of course, this impacts the final spectrum as well, and the 1037.6 Å line is broader than the 1031.9 Å line in the final spectrum shown in Figure 1, though the magnitude of the discrepancy is reduced. It is alternatively possible that the O VI λ 1031.9 line is artificially narrow due to noise or an unrecognized warm pixel which fills in the profile somewhat – we cannot rule out or favor any of these possibilities with the current STIS data. Consequently, we provide below results from measurement of the 1031.9 Å line only as well as results from measurement of both O VI lines.

2.2. WIYN Galaxy Redshift Measurements

As part of our continuing study of the relationship between low z Ly α absorbers and galaxies (see Tripp, Lu, & Savage 1998), we have also measured the redshifts of galaxies in the $\sim 1^\circ$ field centered on PG 0953+415 with the fiber-fed multiobject spectrograph (Hydra, see Barden & Armandroff 1995) on the WIYN telescope. The observations and measurement techniques are described in Tripp et al. (1998), and the new redshifts will be provided in a subsequent paper. Here we note that this survey has revealed four galaxies within ~ 130 km s $^{-1}$ of the O VI absorber at $z_{\text{abs}} = 0.14232$. The measured redshifts of these galaxies are summarized in Table 1 along with some of their properties including projected distance from the sight line (ρ), velocity displacement from the absorber, and O and E magnitudes from the revised APS digitization of the POSS I plates (Pennington et al. 1993). We also list B_J magnitudes calculated using the relation between O_{APS} and B_J derived by Odewahn & Aldering (1995) and the corresponding absolute magnitudes in Table 1. These are all luminous galaxies ranging from $0.6L_*$ to $4.0L_*$ (assuming $M_{B^*} = -19.5$ from Loveday et al. 1992). The velocity dispersion of this group is very uncertain since we do not know the redshift of the group center of mass and because of the small sample. However, if we assume that the O VI absorption arises at the center of mass of the group, then the radial velocity dispersion is roughly 100 km s $^{-1}$, consistent with typical values observed in poor groups (e.g., Zabludoff & Mulchaey 1998).

The spectrum of the galaxy in Table 1 with the smallest projected separation from the sight line ($\rho = 395$ kpc) shows strong Balmer lines in absorption as well as the other usual absorption lines, e.g., Ca II H & K, and well detected [O II] and H β emission lines with observed equivalent widths of 10.5 ± 2 Å and 4.5 ± 0.5 Å, respectively. However, the [O III] emission lines are not apparent (H α is redshifted beyond the red end of the spectrum). Based on its luminosity and the Kennicutt (1992a,b) atlas of integrated galaxy spectra,

Table 1. Galaxies within $\sim 130 \text{ km s}^{-1}$ of the O VI Absorber

Galaxy Redshift ^a	ρ^b (Mpc)	Δv^c (km s^{-1})	R.A. ^d (J2000)	Decl. ^d (J2000)	O_{APS}^e	$(O - E)_{\text{APS}}^e$	B_J^f	M_B^g
0.14280	0.395	126	9 56 38.90	41 16 46.6	18.4	1.3	17.9	-21.0
0.14282	1.00	131	9 57 21.41	41 20 17.3	19.0	1.4	18.5	-20.4
0.14257	2.38	66	9 58 15.07	41 23 23.8	20.4	2.5	20.0	-18.9
0.14274	3.00	110	9 55 14.17	41 3 23.3	19.1	0.6	18.6	-20.3

^aInternal redshift errors are estimated to be $\sim 50 \text{ km s}^{-1}$.

^bProjected distance to the sight line (impact parameter) assuming $H_0 = 75 \text{ km s}^{-1} \text{ Mpc}^{-1}$ and $q_0 = 0.0$. The QSO coordinates (J2000) are R.A. = $9^{\text{h}}56^{\text{m}}52^{\text{s}}.4$, decl. = $+41^{\text{d}}15'22''.0$.

^c $\Delta v = c(z_{\text{gal}} - z_{\text{abs}})/(1 + z_{\text{mean}})$ where z_{mean} is the mean of z_{abs} and z_{gal} .

^dUnits of right ascension are hours, minutes, and seconds, and units of declination are degrees, arcminutes, and arcseconds.

^ePOSS I O and E magnitudes from the revised APS catalog (Pennington et al. 1993), see <http://aps.umn.edu>.

^f B magnitude calculated from the relation derived by Odewahn & Aldering (1995): $O_{\text{APS}} - 18 = 0.96(B_J - 18) + 0.52$.

^gAbsolute magnitude calculated using the interstellar extinction correction based on $E(B - V)$ from Lockman & Savage 1995 and the K -correction $K = 2.5 \log(1 + z)$.

this implies that the galaxy is a normal Sb-Sc spiral or a peculiar S0-Sa galaxy, without an active nucleus. The galaxy at $\rho = 3.0$ Mpc is also an emission line galaxy with [O II], [O III], $H\beta$, and even $H\gamma$ seen in emission. This object has strong emission lines; the observed [O II] equivalent width is 37 ± 10 Å. There are no indications of an active nucleus (e.g., broad $H\beta$ or large [O III]/ $H\beta$ ratios), so given its high luminosity we classify this galaxy as a starbursting spiral or a normal Sc-Sd spiral. The other galaxies in Table 1 do not have emission lines and cannot be unambiguously classified.

It is important to note that the galaxy redshift survey we have been able to carry out to date is not very complete except at relatively bright limiting magnitudes, and it is quite possible that there are additional galaxies at $z \approx 0.142$ which are closer to the sight line than those in Table 1. Consequently, we cannot comment on whether or not a dwarf galaxy could give rise to the O VI system, for example. As we shall discuss in §5.1, it is difficult to discriminate between the hypothesis that the O VI absorption originates in an intragroup medium and the hypothesis that it occurs in the ISM of an individual galaxy given the limited information currently available. More galaxy redshift measurements and deep imaging would be valuable.

3. Absorption Line Measurements

The absorption line profiles of the O VI and H I Ly α lines at $z_{\text{abs}} = 0.14232$ are plotted versus restframe velocity in Figure 3. This figure also shows the spectral regions of lines of interest which are not detected. Restframe equivalent widths (W_r) of the O VI and H I absorption lines were measured using the software of Sembach & Savage (1992), but adapted to use the statistical uncertainties directly calculated from the signal and background counts recorded by STIS. This software accounts for errors due to uncertainty in the height and curvature of the continuum as well as a 2% uncertainty in the flux zero point in the overall uncertainty in W_r [see the appendix in Sembach & Savage (1992) for details]. These equivalent widths are listed in Table 2. This software was also used to set upper limits on the N V, Si III, Si II, and C II equivalent widths, which are also listed in Table 2.

To measure column densities, we have used two methods: the apparent column density technique (e.g., Savage & Sembach 1991) and Voigt profile fitting. For Voigt profile fitting, we have used the software of Fitzpatrick & Spitzer (1997) with the line spread functions for the E140M mode with the $0.2 \times 0.2''$ aperture shown in Figure 13.87 of the Cycle 9 STIS Handbook. This software provides Doppler parameters (b), velocities (v), and column densities (N) for a number of components which is subjectively specified by the user. The

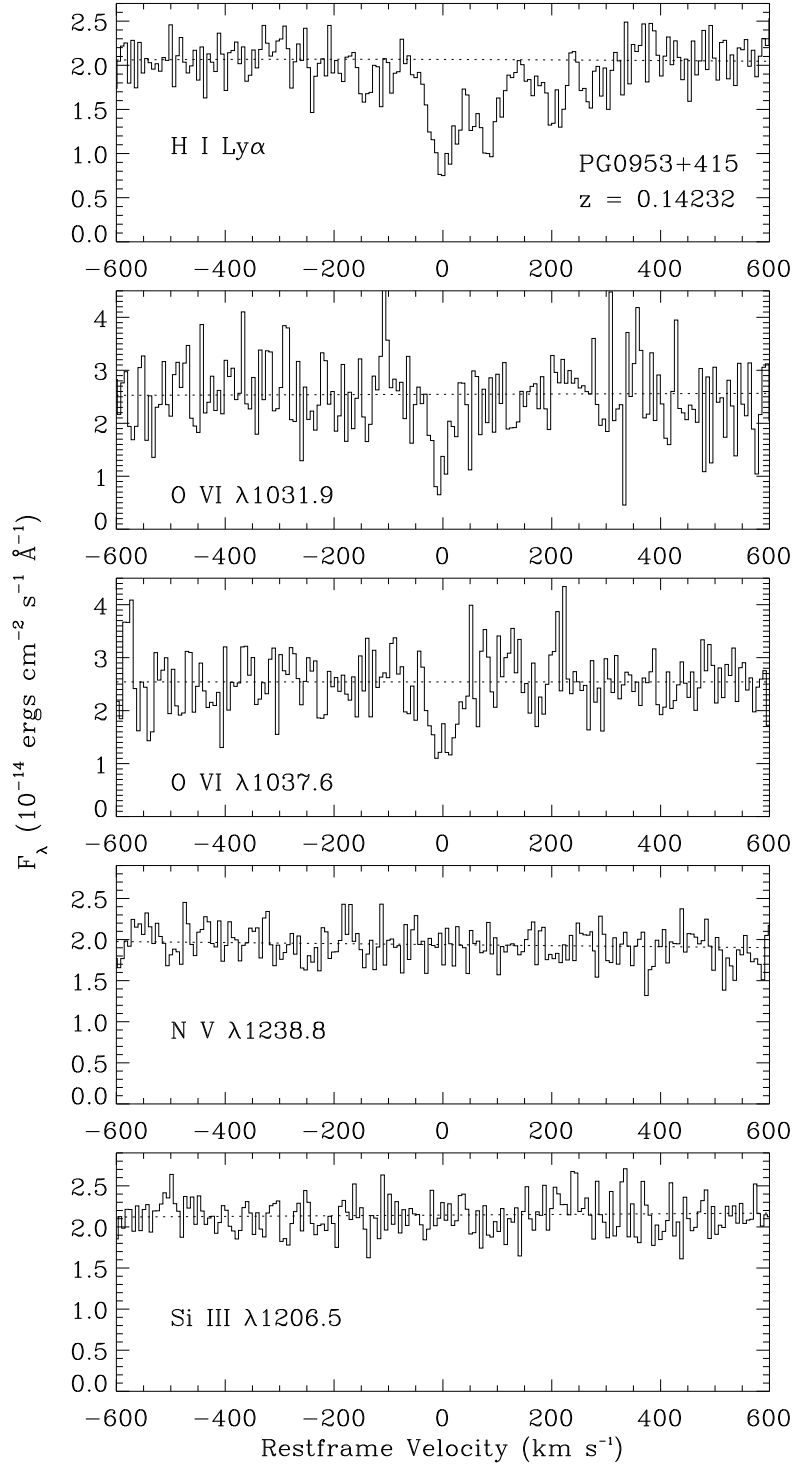


Fig. 3.— Absorption line profiles of the O VI and H I Ly α lines at $z_{\text{abs}} = 0.14232$, plotted versus restframe velocity. The dotted lines show the continua adopted for equivalent width and apparent column density measurements as well as profile fitting (see text §3). Spectral regions of lines of interest which are *not* detected are shown in the lower panels. In this figure, the data have been binned two pixels into one (for display purposes only).

Table 2. Equivalent Widths and Integrated Column Densities of the O VI Absorber at $z = 0.14232$

Species	λ_0^a (Å)	W_r^b (mÅ)	$\log N_a^c$	v_- (km s ⁻¹)	v_+ (km s ⁻¹)
H I	1215.67	423±28	14.00±0.03	-175	330
O VI	1031.93	84±15	14.04 ^{+0.10} _{-0.13}	-40	40
O VI	1037.62	97±15	14.35 ^{+0.08} _{-0.10}	-40	40
N V	1238.80	<36 ^d	<13.2 ^d	-40	40
Si IV	1393.76	<69 ^d	<12.9 ^d	-40	40
Si III	1206.50	<41 ^d	<12.3 ^d	-40	40
Si II	1304.37 ^e	<27 ^d	<13.3 ^d	-40	40
C II	1334.53	<42 ^d	<13.3 ^d	-40	40
C IV	1548.20	<280 ^f	<13.8 ^g

^aRestframe vacuum wavelength from Morton (1991). Oscillator strengths used for these measurements were also obtained from Morton (1991).

^bRestframe equivalent width integrated from v_- to v_+ . This velocity range includes all readily apparent components (see Figure 2).

^cApparent column density (see text) integrated from v_- to v_+ .

^d 4σ upper limit.

^eThe strongest Si II line at 1260.42 Å is recorded in a region of the spectrum affected by the FUV MAMA repeller wire, so we elected to use the Si II λ 1304.37 line instead. In the wavelength range covered by the STIS spectrum, the Si II lines at 1190.42 and 1193.29 Å are expected to be stronger than the 1304.37 Å line, but these lines have unreliable oscillator strengths (see §3.2.1 in Tripp, Lu, & Savage 1996).

^f 4σ upper limit from the Faint Object Spectrograph observations reported by Jannuzi et al. (1998).

^gThe 4σ upper limit for $\log N(\text{C IV})$ obtained assuming unsaturated absorption.

Table 3. Velocities, Doppler Parameters, and Column Densities of Individual Components of the $z = 0.14232$ Absorber

Species	λ_0^b (Å)	v^c (km s ⁻¹)	b (km s ⁻¹)	log N
H I	1215.67	-142±3	12 ⁺¹⁵ ₋₇	12.74±0.10
		1±2	31±7	13.59±0.03
		81±2	30±9	13.43±0.04
		163±7	~20 ^d	12.6±0.21
		207±3	19 ⁺¹⁵ ₋₉	13.08±0.08
O VI	1031.92 ^e	269±4	17 ⁺²⁶ ₋₁₀	12.81±0.12
		-3±3	19 ⁺¹³ ₋₈	14.03±0.09
O VI	doublet ^f	-2±2	22 ⁺¹⁰ ₋₇	14.16±0.06

^aIndividual component parameters determined from profile fitting with the software of Fitzpatrick & Spitzer (1997).

^bRestframe vacuum wavelength from Morton (1991). Oscillator strengths used for these measurements were also obtained from Morton (1991).

^cVelocities are in the restframe of the O VI absorber with $v = 0$ km s⁻¹ at $z_{\text{abs}} = 0.14232$.

^dThis parameter is poorly constrained by the profile fitting software; the nominal value at the minimum χ^2 is listed.

^eComponent parameters based on fitting of the O VI $\lambda 1031.92$ line *only*. For the reasons noted in §2.1, this fit is preferred over the fit to both lines of the O VI doublet.

^fComponent parameters based on fitting of *both* lines of the O VI $\lambda\lambda 1031.92, 1037.62$ doublet.

profile fitting results are summarized in Table 3. Since the O VI $\lambda 1037.6$ Å line may be artificially broadened by a noise feature (see §2.1), we present two alternative fits in Table 3: a fit to the O VI $\lambda 1031.9$ line *only* and a fit to both of the O VI lines.

In the apparent column density approach, the apparent column density per unit velocity, $N_a(v)$, is calculated directly from the apparent optical depth,

$$N_a(v) = (m_e c / \pi e^2) (f \lambda)^{-1} \tau_a(v) = 3.768 \times 10^{14} (f \lambda)^{-1} \ln[I_c(v)/I(v)] \quad (1)$$

in atoms $\text{cm}^{-2} (\text{km s}^{-1})^{-1}$, where f is the oscillator strength, λ is the wavelength in Å, $I(v)$ is the observed line intensity and $I_c(v)$ is the estimated continuum intensity at velocity v , and the other symbols have their usual meanings. If the lines are fully resolved or are not affected by saturation, then the total column density can be obtained by simple integration, $N = \int N_a(v) dv$. We used the software of Sembach & Savage (1992) to measure the apparent column densities, so again, uncertainties due to the continuum placement and a 2% uncertainty in the flux zero point are included in the final error bars.

The H I Ly α and O VI $\lambda 1031.9$ $N_a(v)$ profiles are plotted in Figure 4, and their integrated apparent column densities are provided in Table 2. This table also lists 4σ upper limits on column densities of several species of interest obtained by integrating $N_a(v)$ over the velocity range of the undetected lines. We also include a 4σ upper limit on C IV $\lambda 1548.2$ from the Faint Object Spectrograph (FOS) observations of Jannuzi et al. (1998). Figure 4 shows that there appears to be a small velocity difference between the centroid of the strongest component of the H I profile and that of the O VI line. However, the H I and O VI velocities from profile fitting agree within their 1σ uncertainties. More importantly, Figure 4 shows that the main component of the H I profile is broader than the O VI 1031.9 Å line, which suggests that the line widths are (at least partially) controlled by thermal motions (see §4.1). However, it is alternatively possible that the two strongest components of the H I profile include contributions from narrow features which are not detected in the O VI line. Such additional narrow lines, if present, are not well-constrained by the current data.

4. Physical Conditions

We now turn to the physical conditions of the absorbing gas. As discussed in §1, we are especially interested in testing the warm/hot gas prediction of cosmological simulations of structure growth. For this purpose we seek to constrain the gas temperature in §4.1, and we examine the ionization mechanism in §4.2.

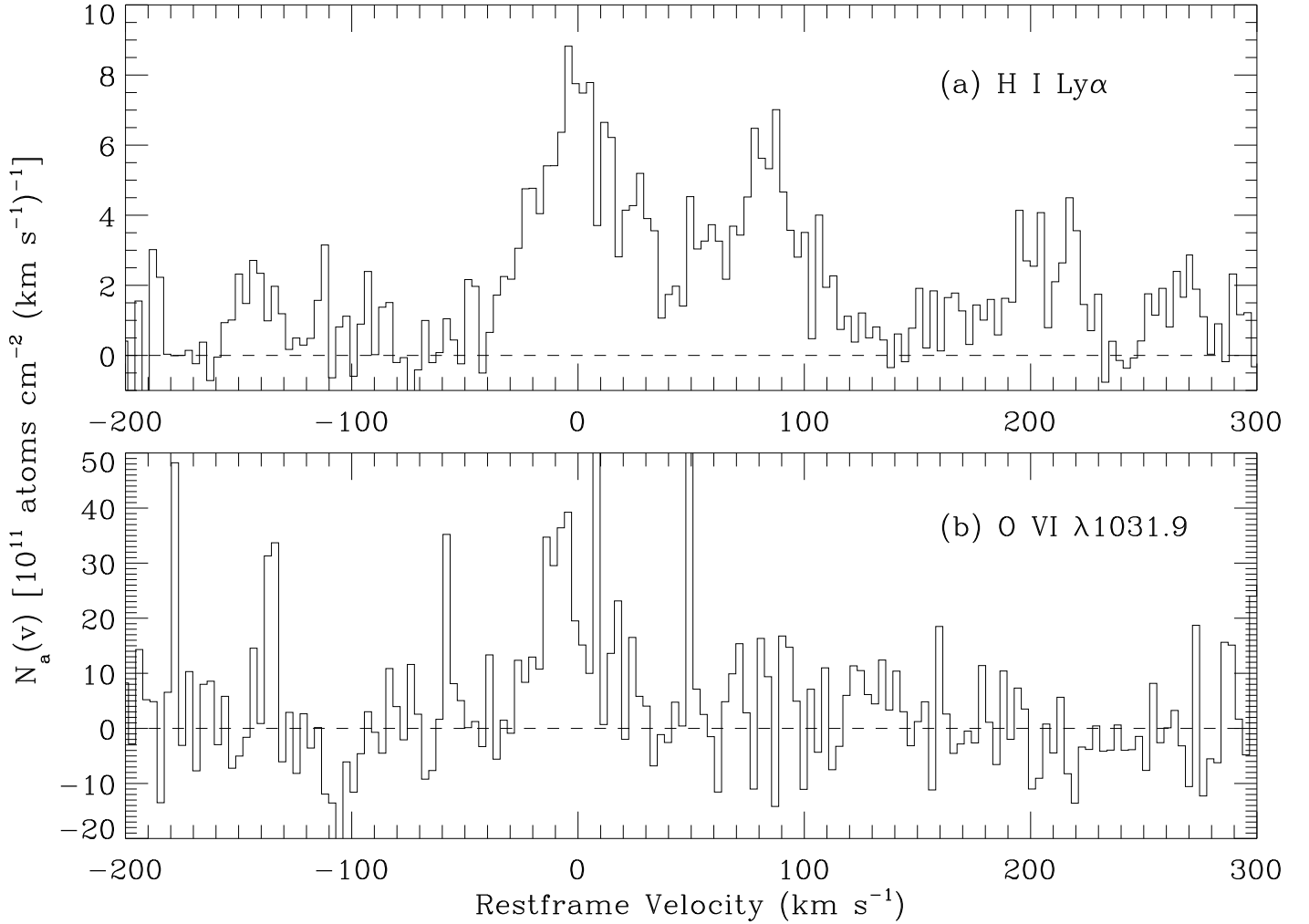


Fig. 4.— Apparent column density profiles (see text §3) of (a) the H I Ly α and (b) O VI λ 1031.9 lines plotted versus restframe velocity where $v = 0$ at $z_{\text{abs}} = 0.14232$. There appears to be a small difference between the velocity centroids of the O VI and the main component of the H I profile. However, the component velocities from profile fitting agree within the 1σ uncertainties (see Table 3). These $N_a(v)$ profiles are constructed from the full resolution, i.e., unbinned, data.

4.1. Gas Temperature

If the line broadening is entirely due to thermal motions, then the gas temperature can be determined from the Doppler parameter of a given line,

$$T = mb^2/2k = A(b/0.129)^2, \quad (2)$$

where m is the mass and A is the atomic mass number of the element, the Doppler parameter b is in km s^{-1} , and T is in $^\circ\text{K}$. However, it is usually true that additional factors such as gas turbulence or multiple unresolved components contribute to the width of a line, and consequently the gas temperature from equation (2) must be treated as an upper limit. If lines of two or more elements with adequately different masses are available, then b can be expressed as

$$b^2 = b_{nt}^2 + (0.129)^2 T/A, \quad (3)$$

which can be solved for T and b_{nt} , the component of the broadening due to non-thermal motions, assuming the different absorption lines arise in the same gas and that the non-thermal motions (turbulence) can be assumed to have a Gaussian profile.

The temperature upper limits implied by equation (2) and the Doppler parameters in Table 3 are $T(\text{O VI}) \leq 3.5 \times 10^5 \text{ }^\circ\text{K}$ and $T(\text{H I}) \leq 5.8 \times 10^4 \text{ }^\circ\text{K}$ for the strongest component of the H I profile, which is also the closest component to the O VI line in velocity space (see Figure 4). Since the velocity centroids of the O VI and the H I are quite close and, in fact, in agreement within the 1σ error bars, it is plausible that these O VI and H I lines originate in the same gas. Adopting this assumption, we derive from equation (3) $T = 3.9 \times 10^4 \text{ }^\circ\text{K}$ and $b_{nt} = 18 \text{ km s}^{-1}$.

While such low temperatures clearly favor photoionization (see below), we must bear in mind that there are considerable uncertainties in the Doppler parameters. For example, for the strongest component of the H I profile, increasing the b -value in Table 3 by just 1σ increases the upper limit on $T(\text{H I})$ to $8.7 \times 10^4 \text{ }^\circ\text{K}$, much closer to the temperature range where O VI can be produced by collisional ionization. This issue is exacerbated by the non-uniqueness of the fitted profile when dealing with multiple blended components, i.e., assuming a different number of components or a different mix of broad and narrow components can lead to substantially different b -values. We provide an example of this in §4.2.2. It is also possible that the absorption arises in non-equilibrium collisionally ionized gas in which cooling is faster than recombination (see §4.2.2).

4.2. Ionization

Given the measurements in the previous sections, can we favor photoionization or collisional ionization in this O VI absorber? In the Milky Way ISM, O VI likely traces collisionally ionized hot gas (Jenkins 1978a,b), at least in the disk and lower halo. However, in extragalactic O VI absorbers, the EUV ionizing radiation field may be substantially harder, and the absorption might arise in very low density gas with a long path length. Both of these factors make photoionization more viable in the extragalactic case. We first consider the plausibility of photoionized models (§4.2.1), and then we test the collisional scenario (§4.2.2).

4.2.1. Photoionization

We have explored the photoionized scenario using CLOUDY (version 90.04; Ferland et al. 1998) with the standard assumptions, in particular that there has been time for thermal and ionization equilibrium to prevail (see below). The absorber is treated as a constant density plane-parallel slab photoionized by the extragalactic radiation from QSOs and AGNs, as calculated by Haardt & Madau (1996) for $z \approx 0.12$. We set the mean intensity at the H I Lyman limit to $J_\nu(\text{LL}) = 1 \times 10^{-23} \text{ ergs s}^{-1} \text{ cm}^{-2} \text{ Hz}^{-1} \text{ sr}^{-1}$, a value in agreement with observational constraints (e.g., Kulkarni & Fall 1993; Maloney 1993; Tumlinson et al. 1999) and theoretical expectations (Shull et al. 1999). With these assumptions, we varied the metallicity¹⁰ and ionization parameter ($U = n_\gamma/n_{\text{H}} = \text{H ionizing photon density/total hydrogen number density, neutral + ionized}$) to search for models which are consistent with the constraints set above: the H I and O VI column densities, limits on various column density ratios which can be derived using the upper limits in Table 2, and the gas temperature. The *relative* heavy element abundances (e.g., [N/O]) were initially set to the solar values from Grevesse & Anders (1989) and Grevesse & Noels (1993), then we considered an alternative N/O abundance (see below).

The basic results of the photoionization modeling are encapsulated in Figure 5. This figure shows various column density ratios involving O VI and other high ions of interest, plotted as function of the ionization parameter (bottom axis) and n_{H} (top axis). A metallicity of $Z = 1/10 Z_\odot$ was used to construct this model, but at low metallicities

¹⁰We express the linear abundance of element X relative to element Y as (X/Y) and the logarithmic abundance in the usual fashion, $[X/Y] = \log(X/Y) - \log(X/Y)_\odot$, and we indicate the overall metallicity with the variable Z .

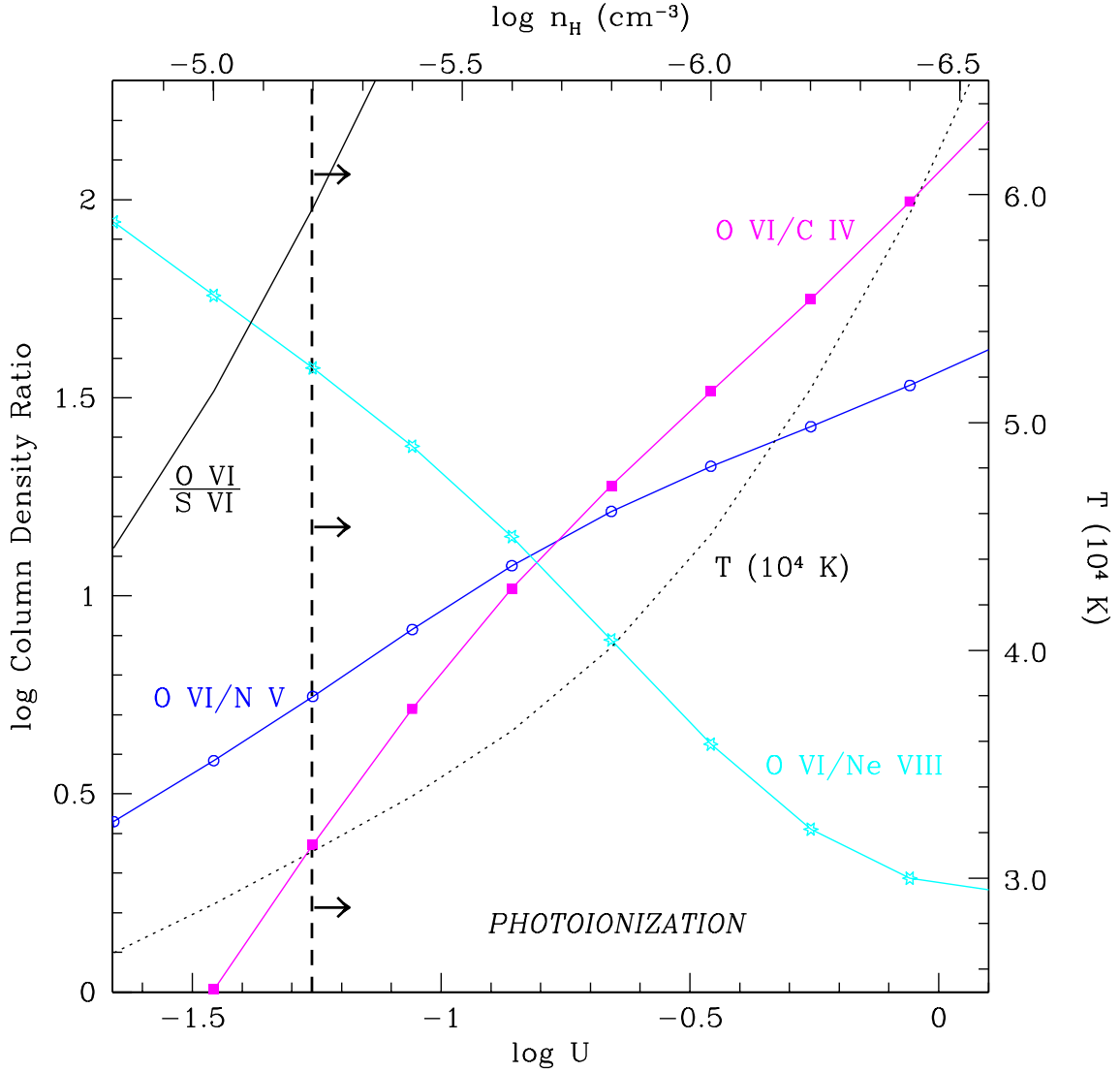


Fig. 5.— Photoionization model calculations of logarithmic ratios of the column densities of O VI to N V (open circles), O VI to C IV (filled squares), and O VI to Ne VIII (open stars) plotted versus the ionization parameter (bottom axis) and the hydrogen number density (top axis). The temperature of the model as a function of the ionization parameter is also shown with a dotted line using the linear scale on the right axis (which is in units of 10^4 °K). The observational lower limit on $N(\text{O VI})/N(\text{N V})$ requires $\log U \geq -1.26$, i.e. only the region of the plot to the right of the vertical dashed line is in agreement with this observational constraint.

the column densities scale nearly directly with Z .¹¹ The gas temperature of the model as a function of U is also indicated by a dotted line in Figure 5 with the linear temperature scale on the right axis. Of the various species that we are able to place limits on using the STIS E140M spectrum (see Table 2), only N V usefully constrains the photoionization model assuming $[N/O] = 0$; when the lower limit on $N(\text{O VI})/N(\text{N V})$ is satisfied, the other species covered in the STIS E140M spectrum are predicted to have undetectably small column densities. Note that the STIS spectrum does not cover the C IV doublet at this redshift, and we discuss the constraint set by the FOS upper limit on C IV below. The O VI/N V column density ratio requires $\log U > -1.26$. Given this limit on U , the photoionized model requires $n_{\text{H}} \leq 10^{-5.2} \text{ cm}^{-3}$ and $T \geq 31,200 \text{ }^\circ\text{K}$. At this ionization parameter, the O VI ionization fraction $f(\text{O VI}) = \text{O VI}/\text{O}_{\text{total}} = 0.164$, and therefore the path length L through the constant density absorbing region must be greater than $\sim 460 \text{ kpc}$ to produce the observed O VI column density, $\log N(\text{O VI}) = 14.04$, in 1/10 solar metallicity gas. With such a long path length, expansion of the universe should lead to an O VI line which is broader than the 1031.9 \AA line shown in Figure 4, and the photoionized model predicts a substantially larger H I column density than observed. While the narrowness of the O VI line may be due to noise, the incorrect $N(\text{H I})$ rules out the 1/10 solar metallicity photoionized model. To match the observed $N(\text{O VI})$ and $N(\text{H I})$ with $\log U = -1.26$ and $J_{\nu}(\text{LL}) = 10^{-23} \text{ ergs}^{-1} \text{ s}^{-1} \text{ cm}^{-2} \text{ Hz}^{-1} \text{ sr}^{-1}$, the photoionization model requires $Z \sim 1.6Z_{\odot}$ and $L \sim 25 \text{ kpc}$, which also alleviates the problem with Hubble broadening and the width of the line. While this is an uncomfortably high metallicity to require, recent *ASCA* observations of X-ray bright galaxy groups indicate that in some groups, the intragroup gas metallicity is $\sim 1/3$ – $1/2$ solar (Davis, Mulchaey, & Mushotzky 1999; Hwang et al. 1999), so this may be marginally plausible. However, in such intragroup gas collisional ionization should be important.

Are these reasonable physical properties? Observations have established that some QSO absorbers can be quite extended. For example, the characteristic Ly α absorber “size” inferred from close QSO pairs is several hundred kpc at moderate redshifts (e.g., Dinshaw et al. 1995; Fang et al. 1996), and this is consistent with cosmological simulations of structure formation (e.g., Rauch, Haehnelt, & Steinmetz 1997; Davé et al. 1999). However, as various authors have argued on different grounds, these large absorbers are likely filamentary structures composed of smaller clouds rather than a single monolithic gas cloud (e.g., Rauch, Weymann, & Morris 1996; Cen & Simcoe 1997). Cen & Simcoe report that individual clouds have sizes of $\sim 50 \text{ kpc}$. Therefore the path length required by the

¹¹As Z approaches the solar value, the increased cooling provided by the metals affects T and, in turn, the ionization balance of the gas.

photoionized model, $L \sim 25$ kpc, is reasonable. The low densities inferred for the O VI absorber at $z_{\text{abs}} = 0.14232$ are also consistent with cosmological simulations: according to equation (2) in Davé et al. (1998), the strongest component of the $z_{\text{abs}} = 0.14232$ absorber is expected to have $n_{\text{H}} \approx 10^{-5.2} \text{ cm}^{-3}$ based on its measured H I column density. Such low densities are also possible in the outer halo of a galaxy like the Milky Way. Murali (2000) has recently argued that the existence of the Magellanic Stream requires $n_{\text{H}} \lesssim 10^{-5} \text{ cm}^{-3}$ in the Milky Way halo at a Galactocentric distance of ~ 50 kpc. Evidently, the size and density of this O VI absorber inferred from the photoionized model are plausible.

The most problematic property of the photoionized model is the required metallicity, $Z \sim 1.6Z_{\odot}$. Most environments in which high metallicities are expected should involve collisional ionization or else should have substantially higher H I column densities. If we use expression (7) from Davé et al. (1999) to estimate the approximate overdensity associated with the $z_{\text{abs}} = 0.14232$ absorber based on its observed $N(\text{H I})$, we find that $\rho_{\text{H}}/\bar{\rho}_{\text{H}} \sim 20$. Based on this overdensity, the cosmological simulations of Cen & Ostriker (1999b) predict that the metallicity of this absorber should be $Z \sim 0.1Z_{\odot}$. Similarly, to produce the absorption in a high metallicity region of the ISM of a galaxy like the Milky Way, the H I column density would have to be substantially higher than the observed $N(\text{H I})$.

We note that the H^+ recombination timescale, $t_{\text{rec}}(\text{H}^+) = 1/\alpha(T)n_{\text{e}}$ where $\alpha(T)$ is the recombination coefficient, exceeds the age of the universe by a factor of several at such low densities, and one may wonder if modeling the gas with a photoionization equilibrium code is valid. However, the timescale for the gas to approach equilibrium, $t_{\text{eq}} = [t_{\text{ion}}^{-1} + 2t_{\text{rec}}^{-1}]^{-1}$ where t_{ion} is the photoionization timescale (see Appendix A in Dove & Shull 1994), is vastly shorter than the recombination timescale in the conditions considered here, and photoionization equilibrium is a good approximation for the low density, highly ionized gas (see, e.g., Vedel, Hellsten, & Sommer-Larsen 1994).

A caveat in the photoionization models above is that we have assumed the solar $[\text{N}/\text{O}]$ abundance. If instead we assume $[\text{N}/\text{O}] \sim -1.5$ based on the trend of $[\text{N}/\text{O}]$ vs. metallicity observed in giant extragalactic H II regions (Vila-Costas & Edmunds 1993), then the lower limit on $N(\text{O VI})/N(\text{N V})$ is satisfied at a lower ionization parameter: the model requires $\log U > -1.90$. However, at lower values of U the model predicts that Si III and Si IV are detectable, and in fact in this case the lower limit on $N(\text{O VI})/N(\text{Si III})$ from Table 2 provides a more stringent constraint requiring $\log U > -1.69$ and $n_{\text{H}} \leq 10^{-4.77} \text{ cm}^{-3}$. Similarly, the FOS upper limit on $N(\text{C IV})$ can be used to set tighter constraints on the photoionized model in this case: the $N(\text{O VI})/N(\text{C IV})$ limit requires $\log U > -1.33$ and $n_{\text{H}} \leq 10^{-5.13} \text{ cm}^{-3}$.

4.2.2. Collisional Ionization

We next consider whether the gas could be collisionally ionized. In §4.1 we derived $T \leq 5.8 \times 10^4$ °K for the gas giving rise to the main component of the H I profile (the component at $v \approx 0$ km s⁻¹). According to the collisional ionization equilibrium calculations of Sutherland & Dopita (1993), no O VI is produced by collisional ionization at this temperature, and in fact O II is the dominant ionization stage of oxygen. If we assume that the O VI and H I absorption lines arise in the same gas with the same turbulent broadening, we obtain $T = 3.9 \times 10^4$ °K, which makes collisional ionization seem rather unlikely. However, the absorber could be out of ionization and thermal equilibrium or it could be a multiphase medium, possibilities which are discussed below.

Furthermore, as noted in §4.1, there are substantial uncertainties in the b -values, and the H I Doppler parameter is consistent with gas having $T \approx 1.6 \times 10^5$ °K at the 3σ level. From the O VI Doppler parameter we obtain $T \leq 3.5 \times 10^5$ °K. These temperatures are more in line with collisionally ionized gas. Furthermore, it is entirely possible that the H I profile contains a broad component at $v \sim 0$ km s⁻¹ superposed on a more narrow component. To demonstrate this, we show in Figure 6 two independent fits to the H I Ly α line. The model profile indicated with a solid line is the initial best fit which has the profile parameters summarized in Table 3. The model profile plotted with a dotted line used a very similar initial guess at the component parameters but was forced to include an additional component with the same velocity as the O VI line and $b = 76$ km s⁻¹, the Doppler parameter of H I in gas with $T = 3.5 \times 10^5$ °K and no turbulent broadening. The two profile fits are nearly indistinguishable — by adjusting the parameters of the other components, the profile fitting code is able to compensate for the presence of the broad component to produce a very similar final result. The final column density required by the profile fitting software for the broad hot component is $N(\text{H I}) = 1.4 \times 10^{13}$ cm⁻². Unless the spectrum has very good S/N, it would be easy to miss such a broad hot H I component. Therefore we cannot rule out the possibility that the gas is collisionally ionized on the basis of the H I Ly α profile properties.

Figure 6 is not shown in order to claim that such a broad component is present, but rather to show that it is allowed by the data. However, this exercise clearly shows that if the O VI absorption occurs in hot gas with $T \approx 3 \times 10^5$ °K, then the absorber must be a multiphase medium because cooler gas is required to account for the rest of the H I Ly α absorption including much of the absorption centered at $v \approx 0$ km s⁻¹. Given sufficient sensitivity, metal lines such as C III $\lambda 977.02$ and Si III $\lambda 1206.50$ should be detectable in these cooler phases, but this may require substantial improvement over the current signal-to-noise due to the low H I column densities.

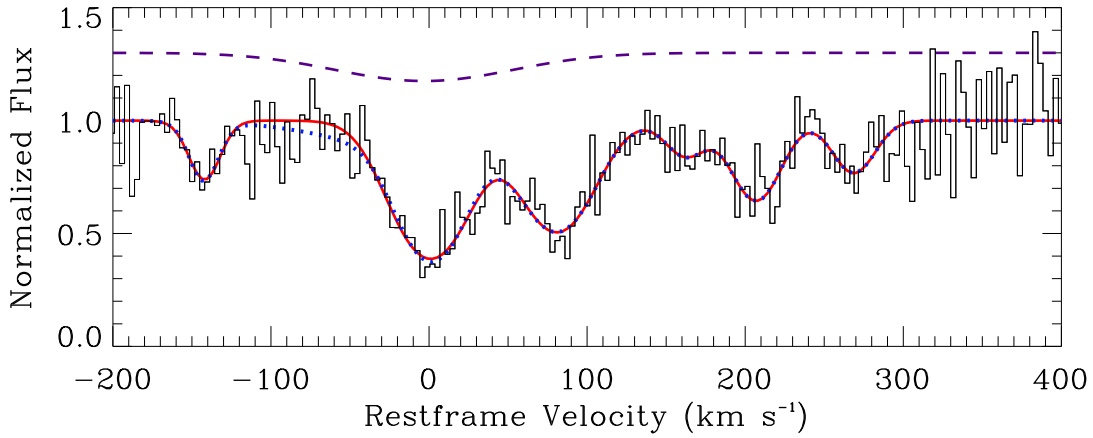


Fig. 6.— Two independent fits to the H I Ly α profile at $z_{\text{abs}} = 0.14232$ (observed spectrum is plotted with a histogram). The solid line shows the initial best-fit with the line parameters in Table 3. The dotted line shows an alternative fit which started with a very similar initial guess at the line parameters but which was forced to include a broad component with a velocity and b -value consistent with hot gas associated with the O VI absorber. This additional broad component is shown with a dashed line offset by 0.3 units above the data. It is very difficult to distinguish between the two fits, and we cannot eliminate the possibility that the H I profile contains a broad component due to hot gas. Note that the STIS data have been plotted at full (i.e., unbinned) resolution in this figure.

We next examine the high ion column density ratios predicted for collisionally ionized hot gas. Several useful high ion column density ratios from the collisional ionization equilibrium calculations of Sutherland & Dopita (1993) are plotted as a function of gas temperature in Figure 7. From this figure we see that if the gas is in collisional ionization *equilibrium*, then T must be greater than 2.3×10^5 °K to satisfy the lower limit on $N(\text{O VI})/N(\text{N V})$, assuming $[\text{N/O}] = 0$. If $[\text{N/O}] = -1.5$, then $T \geq 1.8 \times 10^5$ °K. These are plausible temperatures as discussed above.

However, the temperature range shown in Figure 7 is near the peak of the cooling function, and gas at these temperatures is likely to cool faster than it can recombine, even if it has low metallicity (Sutherland & Dopita 1993), leading to an overionized condition. Consequently, it may be more appropriate to compare the observed ratios to non-equilibrium calculations such as cooling fountain and cluster flow models (e.g., Edgar & Chevalier 1986; Benjamin & Shapiro 2000). Table 4 compares the observed lower limits on the O VI/Si IV, O VI/C IV, and O VI/N V column density ratios in the $z_{\text{abs}} = 0.14232$ absorber to the ratios predicted by non-equilibrium collisionally ionized models including the cooling fountain calculation of Benjamin & Shapiro (2000), the cluster cooling flow model of Edgar & Chevalier (1986), the turbulent mixing layer model of Slavin, Shull, & Begelman (1993), and the magnetized thermal conduction interface modeled by Borkowski, Balbus, & Fristrom (1990). From this table we see that the cooling fountain and conductive interface models are fully consistent with the current observational constraints on this absorber given the right choice of model parameters. The turbulent mixing layer is marginally inconsistent with the O VI/C IV limit, but this should be confirmed with higher sensitivity observations of $N(\text{C IV})$. However, we note that if the turbulent mixing layer post-mixing gas temperature is increased, then the model ironically becomes inconsistent with the O VI/Si IV limit as well, presumably due to increased production of Si IV by self-photoionization.

Given the available observational data, it is difficult to definitively constrain the ionization mechanism. It would be interesting to search for the Ne VIII $\lambda\lambda$ 770.41, 780.32 doublet in O VI absorbers. From Figures 5 and 7, one can see that in the equilibrium ionization models, $\text{O VI}/\text{Ne VIII} \gg 1$ unless the gas has rather low density (in the photoionized case) or is relatively hot (if collisionally ionized). On the other hand, $N(\text{O VI}) \sim N(\text{Ne VIII})$ in the non-equilibrium cooling fountain model (Table 4). Therefore detection of Ne VIII would provide evidence in favor of non-equilibrium collisional ionization. Given sufficient z , the Ne VIII doublet will be redshifted into the bandpass of the *Far Ultraviolet Spectroscopic Explorer* or even the STIS λ range. Unfortunately, $z_{\text{abs}} = 0.14232$ is inadequate, and the Ne VIII doublet is unobservable in this system. It is possible to look for the S VI $\lambda\lambda$ 933.38, 944.52 doublet at $z_{\text{abs}} = 0.14232$ with *FUSE*. However, in most

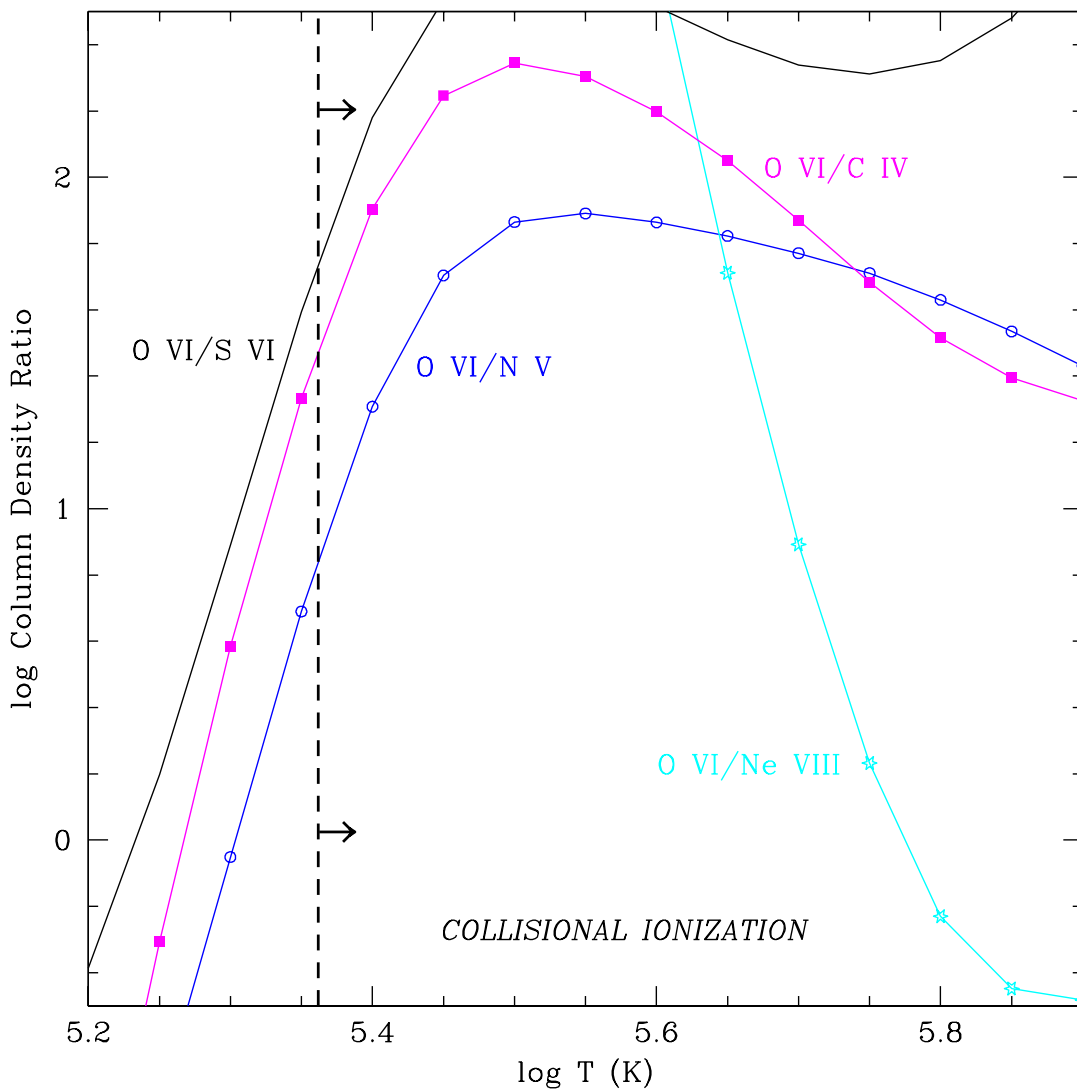


Fig. 7.— Logarithmic high ion column density ratios expected in hot collisionally ionized gas according to the equilibrium calculations of Sutherland & Dopita (1993): O VI/N V (open circles), O VI/C IV (filled squares), and O VI/Ne VIII (open stars). The ratios are plotted versus gas temperature. The observational lower limit on $N(\text{O VI})/N(\text{N V})$ requires $\log T \geq 5.36$, i.e. only the region of the plot to the right of the vertical dashed line is in agreement with this observational constraint.

Table 4. Comparison of High Ion Ratios to Non-Equilibrium Collisionally Ionized Models

Column Density Ratio	Observed Limit ^a	Cooling Fountain ^b	Cluster Cooling Flow ^c	Mixing Layer ^d	Conductive Interface ^e
O VI/Si IV	>13.8	6.2 – 49	66 – 180	17 – 19	39 – 210
O VI/C IV	>1.6 ^f	2.0 – 10	5.7 – 14	0.7 – 0.7	1.4 – 4.5
O VI/N V	>5.5	13 – 23	14 – 21	7.6 – 7.6	4.1 – 7.4
O VI/S VI ^g	...	120 – 140	92 – 104	...	44 – 81
O VI/Ne VIII ^h	...	1.4 – 2.4

^aBased on the data in Table 2 unless otherwise indicated.

^bCooling fountain model from Benjamin & Shapiro (2000), including self-photoionization, for gas initially heated to 10^6 °K.

^cCluster cooling flow model from Edgar & Chevalier (1986) for the isochoric and $T_{\text{tr}} = 2.2 \times 10^5$ °K cases.

^dTurbulent mixing layer ratios calculated by Slavin et al. (1993) for entrainment velocities of 25–100 km s⁻¹, a post-mixing gas temperature of $10^{5.0}$ °K, and no dust depletion (see their Table 4A).

^eThermal conduction front model from Borkowski et al. (1990) with an age of $10^{5.2}$ years and magnetic field inclinations ranging from 0 to 60° relative to the front normal (see their Figure 6). Note that in this model, these ratios increase or remain roughly constant as the age exceeds $10^{5.2}$ years.

^fBased on the 4σ upper limit on the C IV equivalent width from Jannuzi et al. (1998), assuming the linear portion of the curve of growth applies. This limit is less conservative than the limits in the third column of Table 2 because it does not account for the uncertainty in the continuum placement.

^gS VI has resonance lines at 933.38 and 944.52 Å which can be observed with the *Far Ultraviolet Spectroscopic Explorer* (Sembach 1999). Unfortunately, at this redshift one of the S VI lines may blend with the Ar I 1066.66 Å resonance line.

^hThe Ne VIII resonance lines are at 770.41 and 780.32 Å and therefore cannot be observed at the redshift of the O VI absorber studied in this paper. However, *FUSE* will be able to look for this doublet in somewhat higher redshift O VI systems such as the one studied by Savage et al. (1998), so we include it here for purposes of illustration (see text).

models this doublet is predicted to be substantially weaker than the O VI lines (see Figures 5 and 7 and Table 4).

5. Discussion

5.1. Association with a Galaxy Group

The fact that the $z_{\text{abs}} = 0.14232$ O VI absorption line system is associated with a group of galaxies strongly indicates that the absorber is an *intervening* system rather than an *intrinsic* absorber which was ejected or somehow accelerated to high displacement velocity by the QSO. While this may seem a trivial conclusion since the O VI is displaced from the QSO redshift by $\sim 23,000 \text{ km s}^{-1}$, during the last few years observations of absorption variability have established that some highly ionized intrinsic QSO absorbers are separated from z_{QSO} by such large velocities (e.g. Hamann, Barlow, & Junkkarinen 1997) and yet are relatively narrow (i.e., not traditional broad absorption line outflows). Therefore, it is important to find evidence that a given O VI absorber is indeed intervening even if Δv is large. Of course, this association with a galaxy group does not necessarily indicate that the absorption arises in the intragroup medium; it could be due to gas within one of the galaxies in the group. We briefly discuss some possibilities below.

The close proximity of the O VI system to a galaxy group provides a theoretical prejudice in favor of collisional ionization. The presence of galaxies requires that intergalactic gas has collapsed in this region of space, and simple arguments (e.g., §3 in Cen & Ostriker 1999a) suggest that substantial shock-heating probably occurred as a result. Therefore collisionally ionized gas is expected in the vicinity (if not along the pencil-beam probed by the QSO). It is interesting that this absorption system and associated galaxies fit the prediction of Mulchaey et al. (1996) discussed in §1: a group which is possibly spiral-rich and has associated O VI absorption, as expected based on their postulated collisionally ionized intragroup medium. However, we really are not sure that this is a spiral-rich group (or even a bound group) with only four known galaxies, and it is also possible that the O VI absorption arises in the gaseous halo of a single galaxy. However, models of galaxy gaseous halos (e.g., Mo & Miralda-Escudé 1996) also usually produce O VI absorption in a collisionally ionized hot phase. Similarly, models which produce QSO absorption line gas in supernova-driven winds from dwarf galaxies (e.g. Wang 1995) also involve substantial shock-heating and collisionally ionized gas.

The kinematics of the absorption also provide useful information about the possible origins of the system at $z_{\text{abs}} = 0.14232$. A fundamental question is whether the absorption is

due to the intragroup medium or to the ISM of a single galaxy that happens to intercept the line-of-sight. The H I Ly α profile has the “leading edge asymmetry” that various authors (e.g., Lanzetta & Bowen 1992) have discussed as the signature of a moderately edge-on rotating disk. Of course, this is not a unique interpretation of such profile asymmetry, but it provides some evidence in favor of the single-galaxy interpretation. The simplicity of the O VI profile also favors this interpretation. The velocity dispersion of poor galaxy groups is typically one to a few hundred km s $^{-1}$ (Zabludoff & Mulchaey 1998), so one might expect the O VI to be spread over a larger velocity range if the absorption is due to the intragroup medium. Here, though, we must recognize that the observed O VI profiles are noisy and we only detect O VI at the velocity of the *strongest* component of the H I profile. If the hot gas is concentrated at the center of the group, then this may be the only location along the line-of-sight where we have sufficient sensitivity to detect it, and there may be O VI absorption at other velocities which has fallen below our detection threshold. To sort out the various possibilities, it would be very helpful to obtain additional STIS observations to improve the signal-to-noise and search for O VI at other velocities.

5.2. Number Density and Cosmological Mass Density

One means to test the warm/hot gas prediction of cosmological simulations (§1) is to compare the number of O VI absorbers observed per unit redshift, dN/dz , to the number statistically predicted from many random pencil-beams through the cosmological simulations. Is the observed dN/dz consistent with the number predicted by the cosmological models? We can also estimate the mean cosmological mass density traced by the O VI systems at low z .

For these purposes, we combine the STIS observations of PG0953+415 with the GHRS observations of H1821+643 from Tripp et al. (1998).¹² We emphasize that the manner in which these QSOs were selected should not bias the sample to enhance the number of O VI systems detected compared to sampling many random directions. Both QSOs were originally observed to study the relationship between weak Ly α clouds and galaxies¹³ at $z < 0.3$. These two objects were selected for this project simply because they are among the brightest known QSOs with $z > 0.2$, criteria which were required to substantially increase

¹²After this paper was completed, Tripp, Savage, & Jenkins (2000) carried out an analysis of new STIS echelle observations of H1821+643 with the E140M mode, and we refer the reader to that paper for the O VI number density and cosmological mass density derived from an independent data set.

¹³*HST* program IDs 6155 and 7747, see Tripp et al. (1998) for details.

the sample of *weak* Ly α absorbers with a minimal amount of *HST* time. No consideration was given to factors which might indicate an enhanced likelihood of detecting the O VI doublet when the targets were selected.

To estimate dN/dz of the O VI systems, we define a sample of O VI lines with $W_r > 60 \text{ m}\text{\AA}$ for both lines of the doublet,¹⁴ and set the maximum absorber redshift, z_{max} , for each sight line to exclude any absorbers within $|\Delta v| \leq 5000 \text{ km s}^{-1}$ of the QSO redshift and thereby avoid contaminating the sample with associated/intrinsic absorbers which are close to the QSO. One might argue that 5000 km s^{-1} is insufficient (see above). However, we find that the two O VI systems in the final sample are associated with galaxy groups, which suggests that these are indeed intervening absorbers. The lower redshift cutoff for each sight line, z_{min} , was determined by the lowest wavelength in the observed spectrum (with a small buffer to ensure that a line would be recognized if at that λ) in the case of H1821+643 and by the wavelength at which the S/N is unacceptably low in the case of PG0953+415. These criteria resulted in a sample of two O VI absorbers within a total redshift path of $\Delta z = 0.100$ (after a significant correction of 0.067 for regions of the spectra in which we cannot detect either of the O VI lines¹⁵ because they would be blocked by strong ISM or extragalactic lines from other redshift systems). Therefore, $dN/dz \sim 20$ for O VI systems with $W_r \geq 60 \text{ m}\text{\AA}$ at $z < 0.3$. Using the confidence limits from Gehrels (1986) for a sample of two absorbers, we derive $4 < dN/dz < 63$ for these O VI absorbers at the 90% confidence level.

For comparison, Tripp et al. (1998) find $dN/dz = 102 \pm 16$ for H I Ly α lines with $W_r \geq 50 \text{ m}\text{\AA}$ at $z < 0.3$, and Weymann et al. (1998) report $dN/dz = 33 \pm 4$ for Ly α absorbers at $z = 0$ with $W_r \geq 240 \text{ m}\text{\AA}$ based on a large sample at $z < 1.5$. In the case of low to moderate redshift Mg II absorbers, $dN/dz = 0.97 \pm 0.10$ for $W_r \geq 300 \text{ m}\text{\AA}$ (Steidel & Sargent 1992) and $dN/dz = 2.65 \pm 0.15$ for $W_r \geq 20 \text{ m}\text{\AA}$ (Churchill et al. 1999; see also §6 in Tripp, Lu, & Savage 1997). Evidently, these weak low z O VI systems have a substantially larger cross section and/or covering factor than the Mg II absorbers. Similarly, the *stronger* O VI absorbers at higher redshifts are less common: Burles & Tytler (1996) report $dN/dz = 1.0 \pm 0.6$ for O VI systems with $W_r \geq 210 \text{ m}\text{\AA}$ at $\langle z_{\text{abs}} \rangle = 0.9$, and similar results (with smaller uncertainties) are derived from the larger sample provided by the FOS Quasar Absorption Line Key Project (B. Jannuzi & R. Weymann 2000, private communication). This comparison with the O VI dN/dz derived from FOS data must be

¹⁴The 3σ detection limit throughout the region where O VI absorbers can be detected is $60 \text{ m}\text{\AA}$ or better in the spectrum of PG0953+415 and $50 \text{ m}\text{\AA}$ or better in the spectrum of H1821+643.

¹⁵Both of the O VI lines were required to fall in unblocked regions of the spectra so that the doublet could be securely identified.

interpreted carefully, however, because the FOS samples are dominated by lines which are substantially stronger and at substantially higher redshifts than the O VI absorbers discussed in this paper. With a larger sample of low z weak O VI absorbers and smaller uncertainties in their number density, comparison of dN/dz to the space density of objects such as dwarf galaxies may provide insight on the nature of the O VI systems.

Next we estimate the baryonic content of the O VI absorbers, expressed as the cosmological mass density $\Omega_b(\text{O VI})$, following previous analogous calculations for damped Ly α systems (e.g., Lanzetta et al. 1991) as well as O VI absorbers (Burles & Tytler 1996). To estimate the density of baryons in the gaseous component of the universe traced by O VI, we require information about the metallicity of the gas and the O VI ionization fraction, $f(\text{O VI}) = \text{O VI}/\text{O}_{\text{total}}$. In collisional ionization equilibrium, $f(\text{O VI})$ peaks at ~ 0.2 (Sutherland & Dopita 1993), and similarly low peak fractions are predicted by non-equilibrium collisional models (e.g., Shapiro & Moore 1976; Benjamin & Shapiro 2000). The O VI ion fraction is not much larger at peak value in photoionized gas (see appendix). Therefore we will adopt $f(\text{O VI}) \sim 0.2$ to set a lower limit on the baryonic content of the O VI absorbers, and the following calculation is relatively independent of how the gas is ionized or whether or not it is due to the intragroup medium. For the mean cosmic metallicity of the O VI absorbers, it is less clear what value to adopt, but to set a lower limit on $\Omega_b(\text{O VI})$ we should set (O/H) to a high but plausible value. As noted in §4.2.1, Davis et al. (1999) and Hwang et al. (1999) have derived metallicities of 1/3–1/2 solar for intragroup gas in several X-ray bright groups. Therefore we will initially use 1/2 solar metallicity for the calculation of $\Omega_b(\text{O VI})$ and then discuss how it scales with (O/H) . The mean cosmological mass density in the O VI absorbers, in units of the current critical density ρ_c , can be estimated as

$$\Omega_b(\text{O VI}) = \frac{\mu m_{\text{H}} H_0}{\rho_c c f(\text{O VI})} \left(\frac{\text{O}}{\text{H}} \right)_{\text{O VI}}^{-1} \frac{\sum_i N_i(\text{O VI})}{\sum_i \Delta X_i} \quad (4)$$

where μ is the mean atomic weight (taken to be 1.3), $(\text{O}/\text{H})_{\text{O VI}}$ is the assumed mean oxygen abundance by number in the O VI absorption systems, m_{H} is the mass of hydrogen, $N_i(\text{O VI})$ is the total O VI column density and ΔX_i is the absorption distance interval (Bahcall & Peebles 1969) probed to the i th QSO,

$$\Delta X_i = \frac{1}{2} \{ [(1 + z_{\text{max}})^2 - 1] - [(1 + z_{\text{min}})^2 - 1] \} \quad (5)$$

assuming $q_0 = 0$.¹⁶ As in the calculation of dN/dz , we correct ΔX_i for spectral regions blocked by strong lines. Combining the PG0953+415 STIS data and the GHRS observations

¹⁶Over the redshift range probed by the sight lines to PG0953+415 and H1821+643, results are insensitive to the value assumed for q_0 .

of H1821+643 from Tripp et al. (1998) with z_{\min} and z_{\max} set to the same values used for the derivation of dN/dz , we obtain $\Omega_b(\text{O VI}) \gtrsim 0.0006h_{75}^{-1}$ assuming the mean O abundance is 1/2 solar. This is a lower limit not only because $f(\text{O VI})$ and (O/H) were set to their approximate upper limits, but also because we have applied an equivalent width cutoff to define the sample; if O VI absorbers with $W_r \leq 60 \text{ m\AA}$ significantly increase $\sum_i N_i(\text{O VI})$, then the true $\Omega_b(\text{O VI})$ will be higher. Note that $\Omega_b(\text{O VI})$ is inversely proportional to (O/H) . Decreasing the metallicity to 1/10 solar, for example, increases the lower limit on the O VI absorber baryon content to $\Omega_b(\text{O VI}) \gtrsim 0.003h_{75}^{-1}$.

To demonstrate the level of uncertainty in the cosmological mass density estimate due to small number statistics, we can recalculate $\Omega_b(\text{O VI})$ using an alternative expression analogous to equation (9) from Rao & Turnshek (2000),

$$\Omega_b(\text{O VI}) = \frac{\mu m_{\text{H}} H_0}{\rho_c c f(\text{O VI})} \left(\frac{\text{O}}{\text{H}} \right)_{\text{O VI}}^{-1} \left(\frac{dN}{dz} \right) \frac{\langle N_{\text{O VI}} \rangle}{(1+z)} \quad (6)$$

where $\langle N_{\text{O VI}} \rangle$ is the mean O VI column density of the absorption systems in the sample and again we have assumed $q_0 = 0$. The advantage of this alternative expression for $\Omega_b(\text{O VI})$ is that we can employ the Gehrels (1986) small sample statistics to estimate the uncertainty in dN/dz and then propagate the uncertainty into the estimate of $\Omega_b(\text{O VI})$. With $dN/dz = 20_{-13}^{+26}$ and the other parameters set to the values assumed above, we find for the 1/10 solar metallicity case $\Omega_b(\text{O VI}) \gtrsim 0.003_{-0.002}^{+0.004} h_{75}^{-1}$ (error bars are 1σ uncertainties).

Bearing in mind that there is still considerable uncertainty in the lower limit on $\Omega_b(\text{O VI})$ due to the small sample, small redshift path, and uncertain mean metallicity, this preliminary estimate suggests that the O VI absorbers may indeed harbor a significant fraction of the baryons in the universe at low z . The lower limit assuming $(\text{O}/\text{H}) = 1/10$ solar is comparable to the cosmological mass density of stars, H I, and X-ray emitting galaxy group and cluster gas at low redshift (Fukugita, Hogan, & Peebles 1998), for example.

6. Summary

The paper is summarized as follows.

(1) We have observed the low redshift QSO PG0953+415 with the E140M mode of STIS, and this has revealed an O VI absorption line system at $z_{\text{abs}} = 0.14232$. This O VI absorber is highly ionized: multicomponent H I absorption is also detected at this redshift, but no other species are detected in the STIS spectrum including the N V doublet, Si III, and C II.

(2) We have measured galaxy redshifts in the field of the QSO using the WIYN telescope, and there are at least four galaxies within $\sim 130 \text{ km s}^{-1}$ of the O VI absorber with projected distances ranging from 395 kpc to 3.0 Mpc. Two of these galaxies appear to be spiral galaxies.

(3) A review of the observational constraints shows that we cannot definitively assert that the gas is collisionally ionized or photoionized, but photoionization requires an uncomfortably high metallicity which is inconsistent with theoretical expectations. If the gas is collisionally ionized, it is likely that it is not in equilibrium or that it is a multiphase absorber. Non-equilibrium collisional ionization models are consistent with the observations.

(4) Combining the STIS data on PG0953+415 with the high S/N low resolution GHRS observations of H1821+643 from Tripp et al. (1998), we identify two intervening O VI systems over a redshift path Δz of only 0.10. This implies that dN/dz for O VI systems with $W_r > 60 \text{ m\AA}$ and $z < 0.3$ is ~ 20 with a large uncertainty due to the small number of systems so far detected. This represents a large density for metal line systems since dN/dz for Ly α absorbers with $W_r > 50 \text{ m\AA}$ and $z < 0.3$ is 102 ± 16 (Tripp et al. 1998). We stress that the sample should not be biased in favor of O VI detection. If further observations confirm that dN/dz is as large as 20 for O VI systems, then these absorbers may be an important baryon reservoir at low redshift, although this depends on the metallicity of the gas. If the mean metallicity is 1/2 solar, then $\Omega_b(\text{O VI}) \gtrsim 0.0006 h_{75}^{-1}$. However, if the mean metallicity is 0.1 solar, then $\Omega_b(\text{O VI}) \gtrsim 0.003 h_{75}^{-1}$, which is comparable to the baryonic content of other known constituents of the low z universe such as galaxies and gas in galaxy clusters.

This research has made use of software developed by the STIS Instrument Definition Team for the reduction of STIS data, and we thank the STIS team for allowing us to use their software. We also benefitted from the use of CLOUDY, and we are indebted to Gary Ferland for sharing this program in which he has invested years of development effort. Similarly, we extend our thanks to Ed Fitzpatrick for the use of his profile fitting code and to Ken Sembach for his apparent column density software. Valuable comments were provided by Dave Bowen, Romeel Davé, Bruce Draine, Ed Jenkins, John Mathis, and Linda Sparke. We especially appreciate the careful review of the manuscript provided by Jane Charlton which clarified and improved the paper. We also thank Francisco Haardt for private communication of the Haardt & Madau background radiation fields in a convenient digital format, and Buell Jannuzi and Ray Weymann for private communication regarding the number density of O VI systems in the FOS Quasar Absorption Line Key Project. Finally, this research has made use of the APS Catalog of POSS I, which is supported by the NSF, NASA, and the University of Minnesota. The APS databases can be accessed

at <http://aps.umn.edu/>. T. M. T. acknowledges support from NASA through grant NAG5–30110. B. D. S. acknowledges NASA support through grant GO–06499.02–95A from the Space Telescope Science Institute.

A. Maximum Ionization Fraction of O VI

In §5.2 we adopted $f(\text{O VI}) = 0.2$ to set a lower limit on the baryonic content of the O VI absorbers. Intuitively, $f(\text{O VI}) = 1.0$ would seem to set a more conservative lower limit on $\Omega_b(\text{O VI})$. However, as noted in §5.2, O VI is not a preferred ionization stage of oxygen, and in collisionally ionized gas $f(\text{O VI})$ peaks at ~ 0.2 in equilibrium and non-equilibrium calculations.

To evaluate the maximum O VI ionization fraction which can be attained if the O VI is created by photoionization, we have calculated with CLOUDY an O VI ionization fraction grid as a function of the temperature and ionization parameter of a parcel of gas assuming the Haardt & Madau (1996) UV background radiation at $z = 0.12$. To show how $f(\text{O VI})$ depends on T and U , we operated CLOUDY in a different mode than that employed in §4.2.1: instead of allowing CLOUDY to determine the gas temperature given the various heating and cooling processes which are important (as was done in §4.2.1), we fixed the temperature and ionization parameter at particular values in each grid cell and calculated the ensuing $f(\text{O VI})$ for a grid with $3.0 \leq \log T \leq 7.0$ and $-3.5 \leq \log U \leq 0.5$. The resulting grid is shown in Figure 8.

As expected based on previous calculations, when the ionization parameter is low enough so that photoionization is unimportant and O VI only has a significant ionization fraction in gas which is hot enough to be collisionally ionized, Figure 8 shows that $f(\text{O VI})$ has a maximum value of ~ 0.2 at $\log T = 5.5$. On the other hand, when the ionization parameter is high and photoionization dominates, Figure 8 indicates that $f(\text{O VI})$ could be somewhat larger *if the gas is very cool*. However, this is rather unlikely to occur because the photoionization by the UV background which creates the O VI will also heat the gas to $\log T \gtrsim 4$. For example, the CLOUDY model in Figure 5 which satisfies the O VI and N V constraints requires $\log T \gtrsim 4.5$ (see §4.2.1), and with this temperature constraint the maximum $f(\text{O VI})$ is 0.28. Therefore $f(\text{O VI}) = 0.2$ is a reasonable value for placing a lower limit on the baryonic content of O VI absorbers regardless of whether the gas is photoionized or collisionally ionized.

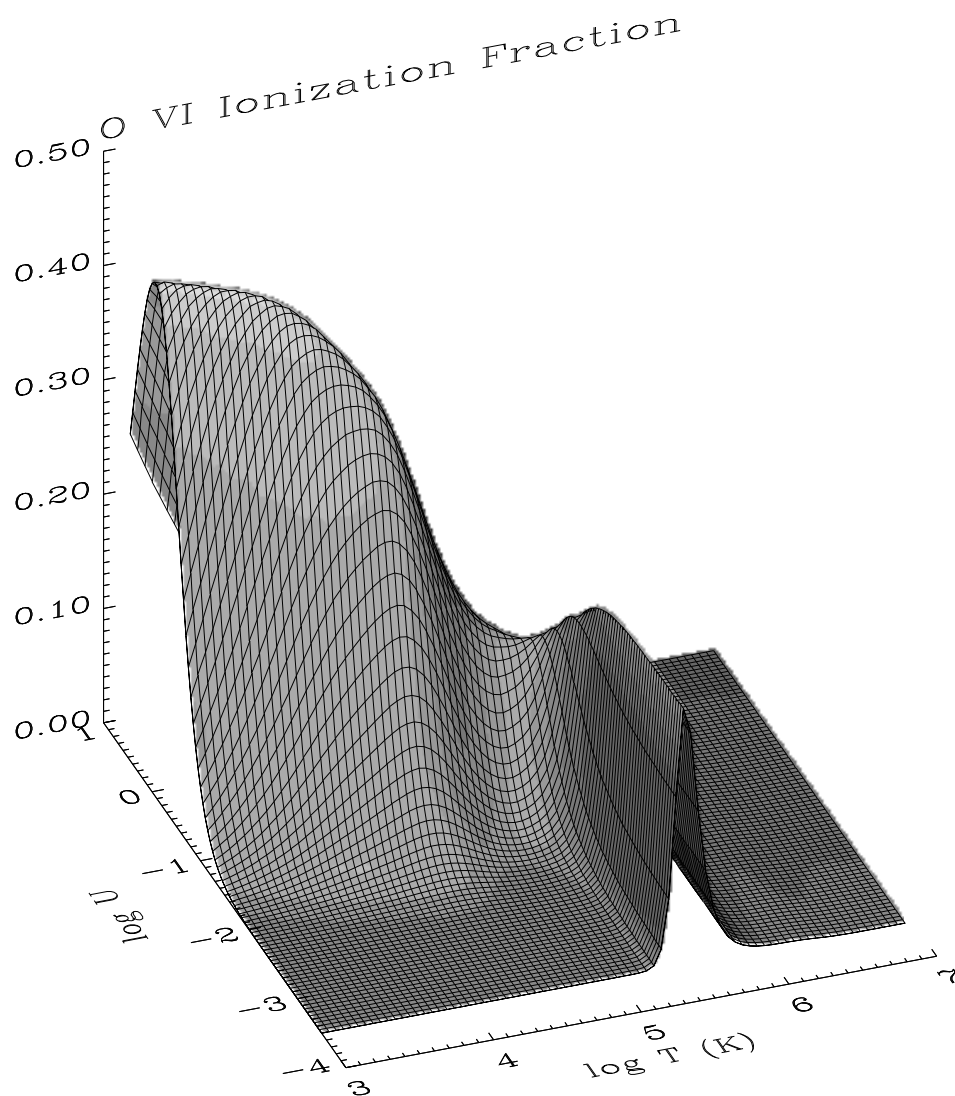


Fig. 8.— Dependency of the O VI ionization fraction, $f(\text{O VI}) = \text{O VI}/\text{O}_{\text{total}}$, of a parcel of gas on the ionization parameter U and gas temperature T , assuming the gas is photoionized by the UV background calculated by Haardt & Madau (1996) at $z \approx 0.12$ (see §4.2.1). It is important to note that U and T were held at fixed values for the calculation of $f(\text{O VI})$ in each cell of this grid to illustrate how the O VI ionization fraction varies with these parameters. However, the low temperature region of this plot is not physically realistic because the photoionization which ionizes oxygen to this degree will also heat the gas to $\log T \gtrsim 4$.

REFERENCES

- Bahcall, J. N., & Peebles, P. J. E. 1969, *ApJ*, 156, L7
- Barden, S. C., & Armandroff, T. 1995, *Proc. SPIE*, 2476, 56
- Benjamin, R. A., & Shapiro, P. R. 2000, *ApJS*, submitted
- Bergeron, J. et al. 1994, *ApJ*, 436, 33
- Blanton, M., Cen, R., Ostriker, J. P., Strauss, M. A., & Tegmark, M. 2000, *ApJ*, 531, 1
- Borkowski, K. J., Balbus, S. A., & Fristrom, C. C. 1990, *ApJ*, 355, 501
- Bowers, C. A., & Lindler, D. 1999, in preparation
- Burles, S., & Tytler, D. 1996, *ApJ*, 460, 584
- Cen, R., & Simcoe, R. A. 1997, *ApJ*, 483, 8
- Cen, R., & Ostriker, J. P. 1999a, *ApJ*, 514, 1
- Cen, R., & Ostriker, J. P. 1999b, *ApJ*, 519, L109
- Churchill, C. W., & Charlton, J. C. 1999, *AJ*, 118, 59
- Churchill, C. W., Rigby, J. R., Charlton, J. C., & Vogt, S. S. 1999, *ApJS*, 120, 51
- Davé, R., Hellsten, U., Hernquist, L., Katz, N., & Weinberg, D. H. 1998, *ApJ*, 509, 661
- Davé, R., Hernquist, L., Katz, N., & Weinberg, D. H. 1999, *ApJ*, 511, 521
- Davis, D. S., Mulchaey, J. S., & Mushotzky, R. F. 1999, *ApJ*, 511, 34
- Dinshaw, N., Foltz, C. B., Impey, C. D., Weymann, R. J., & Morris, S. L. 1995, *Nature*, 373, 223
- Dove, J. B., & Shull, J. M. 1994, *ApJ*, 430, 222
- Edgar, R. J., & Chevalier, R. A. 1986, *ApJ*, 310, L27
- Fang, Y., Duncan, R. C., Crots, A. P. S., & Bechtold, J. 1996, *ApJ*, 462, 77
- Ferland, G. J., Korista, K. T., Verner, D. A., Ferguson, J. W., Kingdon, J. B., & Verner, E. M. 1998, *PASP*, 110, 761
- Fitzpatrick, E. L., & Spitzer, L. 1997, *ApJ*, 475, 623
- Fukugita, M., Hogan, C. J., & Peebles, P. J. E. 1998, *ApJ*, 503, 518
- Gehrels, N. 1986, *ApJ*, 303, 336
- Grevesse, N., & Anders, E. 1989, in *AIP Conf. Proc.* 183, *Cosmic Abundances of Matter*, ed. C. J. Waddington (New York: AIP), 1

- Grevesse, N., & Noels, A. 1993, in *Origin and Evolution of the Elements*, ed. N. Prantzos, E. Vangioni-Flam, & M. Cassé (Cambridge: Cambridge University Press), 15
- Haardt, F., & Madau, P. 1996, *ApJ*, 461, 20
- Hamann, F., Barlow, T. A., & Junkkarinen, V. 1997, *ApJ*, 478, 87
- Hamann, F., & Ferland, G. 1999, *ARA&A*, 37, 487
- Hwang, U., Mushotzky, R. F., Burns, J. O., Fukazawa, Y., & White, R. A. 1999, *ApJ*, 516, 604
- Jannuzi, B. T. et al. 1998, *ApJS*, 118, 1
- Jenkins, E. B. 1978a, *ApJ*, 219, 845
- Jenkins, E. B. 1978b, *ApJ*, 220, 107
- Kennicutt, R. C. 1992a, *ApJ*, 388, 310
- Kennicutt, R. C. 1992b, *ApJS*, 79, 255
- Kimble, R. A., et al. 1998, *ApJ*, 492, L83
- Kingdon, J. B., & Ferland, G. J. 1996, *ApJS*, 106, 205
- Kirkman, D., & Tytler, D. 1997, *ApJ*, 489, L123
- Kirkman, D., & Tytler, D. 1999, *ApJ*, 512, L5
- Kulkarni, V. P., & Fall, S. M. 1993, *ApJ*, 413, L63
- Lanzetta, K. M., & Bowen, D. V. 1992, *ApJ*, 391, 48
- Lanzetta, K. M., Wolfe, A. M., Turnshek, D. A., Lu, L., McMahon, R. G., & Hazard, C. 1991, *ApJS*, 77, 1
- Lopez, S., Reimers, D., Rauch, M. Sargent, W. L. W., & Smette, A. 1999, *ApJ*, 513, 598
- Loveday, J., Peterson, B. A., Efstathiou, G. & Maddox, S. J. 1992, *ApJ*, 390, 338
- Lu, L., & Savage, B. D. 1993, *ApJ*, 403, 127
- Maloney, P. 1993, *ApJ*, 414, 41
- Mihalas, D., & Binney, J. 1981, *Galactic Astronomy* (2d ed.; San Francisco:Freeman)
- Mo, H. J., & Miralda-Escudé, J. 1996, *ApJ*, 469, 589
- Morton, D. C. 1991, *ApJS*, 77, 119
- Mulchaey, J. S., Mushotzky, R. F., Burstein, D., & Davis, D. S. 1996, *ApJ*, 456, L5
- Murali, C. 2000, *ApJ*, 529, L81
- Odehahn, S. C., & Aldering, G. 1995, *AJ*, 110, 2009

- Ostriker, J. P., & Cen, R. 1996, *ApJ*, 464, 27
- Papovich, C., Norman, C., Bowen, D. V., Heckman, T., Savaglio, S., Koekemoer, A. M., & Blades, J. C. 2000, *ApJ*, 531, 654
- Pennington, R. L., Humphreys, R. M., Odewahn, S. C., Zumach, W. A., & Thurmes, P. M. 1993, *PASP*, 105, 521
- Rao, S. M., & Turnshek, D. A. 2000, preprint (astro-ph/9909164)
- Rauch, M., Haehnelt, M. G., & Steinmetz, M. 1997, *ApJ*, 481, 601
- Rauch, M., Weymann, R. J., & Morris, S. L. 1996, *ApJ*, 458, 518
- Savage, B. D., & Sembach, K. R. 1991, *ApJ*, 379, 245
- Savage, B. D., Tripp, T. M., & Lu, L. 1998, *AJ*, 115, 436
- Sembach, K. R. 1999, in *ASP Conference Series Vol. 166, Stromlo Workshop on High-Velocity Clouds*, eds. B. K. Gibson & M. E. Putman, (San Francisco: ASP), 243
- Sembach, K. R., & Savage, B. D. 1992, *ApJS*, 83, 147
- Shapiro, P. R., & Moore, R. T. 1976, *ApJ*, 207, 460
- Shull, J. M., Roberts, D., Giroux, M. L., Penton, S. V., & Fardal, M. A. 1999, *AJ*, 118, 1450
- Slavin, J. D., Shull, J. M., & Begelman, M. C. 1993, *ApJ*, 407, 83
- Steidel, C. C., & Sargent, W. L. W. 1992, *ApJS*, 80, 1
- Sutherland, R. S., & Dopita, M. A. 1993, *ApJS*, 88, 253
- Timothy, J. G. 1994, *Proc. SPIE*, 2209, 372
- Tripp, T. M., Lu, L., & Savage, B. D. 1996, *ApJS*, 102, 239
- Tripp, T. M., Lu, L., & Savage, B. D. 1997, *ApJS*, 112, 1
- Tripp, T. M., Lu, L., & Savage, B. D. 1998, *ApJ*, 508, 200
- Tripp, T. M., Savage, B. D., & Jenkins, E. B. 2000, *ApJ*, 534, L1 (astro-ph/0003277)
- Tumlinson, J., Giroux, M. L., Shull, J. M., & Stocke, J. T. 1999, *AJ*, 118, 2148
- Vedel, H., Hellsten, U., & Sommer-Larsen, J. 1994, *MNRAS*, 271, 743
- Verner, D. A., Tytler, D., & Barthel, P. D. 1994, *ApJ*, 430, 186
- Vila-Costas, M. B., & Edmunds, M. G. 1993, *MNRAS*, 265, 199
- Wang, B. 1995, *ApJ*, 444, L17

Weymann, R. J., et al. 1998, ApJ, 506, 1

Zabludoff, A. I., & Mulchaey, J. S. 1998, ApJ, 496, 39